Measurement of the Index of Refraction of an Aerogel

Tudor Dimofte
Joseph Henry Laboratory, Princeton University, Princeton, NJ 08544

August 2003

Contents

1 Premise

We were confronted with the problem of finding the index of refraction of a certain aerogel. This material is an extremely light SiO_2 glass with a very low index, purportedly as low as 1.007. Indeed, it is sometimes even hard to see. The need to know its index precisely arose from the fact that it will be used in a particle detector. Electrons (and other particles) traveling faster than the speed of light in the aerogel, c/n, will emit observable Cherenkov radiation. The threshold energy that electrons must have for this effect is

$$E_t = \frac{m_e c^2}{\sqrt{1-\beta^2}} \tag{1}$$

with

$$\beta = \frac{v}{c} = \frac{1}{n}, \tag{2}$$

depending explicitly on n; the lower the index, the higher the threshold.

The actual sample of aerogel consisted of four blocks, each roughly $5 \times 5 \times 2$ cm. These blocks were all cut out of one larger ($10 \times 10 \times 2$ cm) block. Unfortunately, only two long adjacent sides of each block were (close to) optically smooth. The two large faces and the other two long sides were cut in such a way that light scattered rather strongly upon passing through them. Laser beams lost their coherency and began spreading. Chances are that the smoother cuts were created when the large initial block was cut into the four smaller ones. Also unfortunate is that one of the four blocks was broken rather badly at the beginning of tests and rendered largely unusable.[1]

Thus we effectively had three samples to work with, each of which had two moderately nice (yet far from perfect) adjacent sides. We tried to measure their index of refraction by two different methods, direct refraction of a laser beam and interferometry.[2] The findings reinforced each other, and in the end we found the index to be

$$n = 1.00955 \pm 0.00013, \tag{3}$$

to the best possible accuracy.

2 Method 1: Refraction

The first method of measuring the index of refraction involved shining a laser beam diagonally through the corner of the aerogel and measuring its deflection, as shown in Figure 1.

Calculating the deflection angle is mostly straightforward. The beam hits the aerogel at angle of incidence γ, refracts once upon entering, and refracts again upon

[1] Aerogel, being an extremely light, stiff glass, is also incredibly fragile.

[2] For both methods, we used a Helium-Neon laser. Techinically speaking, we measured the index of refraction for a wavelength of 632.8 nm.

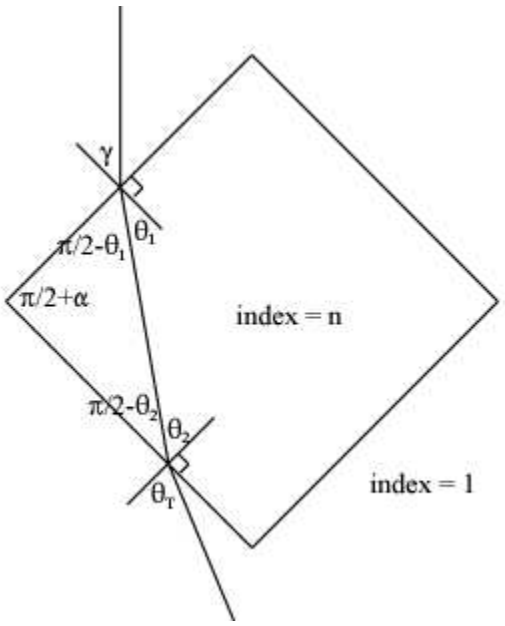

Figure 1: Refraction through a corner

exiting. We assume we don't know the corner angle of the aerogel, and call it $\pi/2+\alpha$ for some small α. With index n, Snell's law gives[3]

$$\begin{aligned} & \sin\gamma = n\sin\theta_1 \\ \Rightarrow \quad & \theta_1 = \sin^{-1}\left(\tfrac{\sin\gamma}{n}\right). \end{aligned} \tag{4}$$

Then from the triangle between the beam and the corner we have

$$\begin{aligned} & \pi = (\pi/2-\theta_1)+(\pi/2-\theta_2)+(\pi/2+\alpha) \\ \Rightarrow \quad & \theta_2 = \pi/2+\alpha-\theta_1, \end{aligned} \tag{5}$$

and again from Snell's law we get

$$\begin{aligned} \theta_T &= \sin^{-1}\left[n\sin\theta_2\right] \\ &= \sin^{-1}\left[n\sin\left(\pi/2+\alpha-\theta_1\right)\right] \\ &= \sin^{-1}\left[n\cos\left(\theta_1-\alpha\right)\right] \\ &= \sin^{-1}\left[n\cos\left(\sin^{-1}\left(\frac{\sin\gamma}{n}\right)-\alpha\right)\right] \\ &= \sin^{-1}\left[\sin\alpha\sin\gamma+\cos\alpha\sqrt{n^2-\sin^2\gamma}\right]. \end{aligned} \tag{6}$$

[3]We are assuming here that the index of the surrounding air is 1. In reality the index of air is about 1.0003, and instead of measuring n we are actually measuring $n/1.0003$. But the difference is sufficiently small to not pose a great problem; the correction is much less than our final error estimate.

Now, the deflection upon entering the aerogel is $\theta_{r1} = \gamma - \theta_1$, and the deflection upon exiting is $\theta_{r2} = \theta_T - \theta_2$. So the total deflection angle of the beam is

$$\begin{aligned}\theta_r &= \theta_{r1} + \theta_{r2} \\ &= \gamma - \theta_1 + \theta_T - \theta_2 \\ &= \gamma - (\pi/2 + \alpha) + \theta_T \\ &= \gamma - (\pi/2 + \alpha) + \sin^{-1}\left[\sin\alpha \sin\gamma + \cos\alpha\sqrt{n^2 - \sin^2\gamma}\right].\end{aligned}$$

Figure 2 shows a plot of $\theta_r(\gamma)$ for $n = 1.0095$ and $\alpha = 0.$[4]

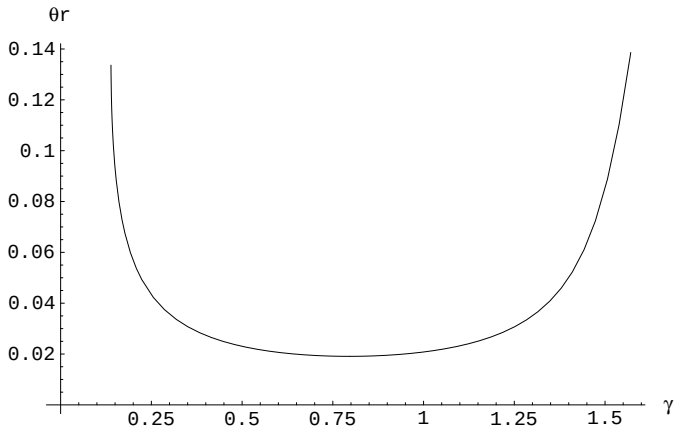

Figure 2: Typical plot of $\theta_r(\gamma)$

2.1 Total internal reflection

The idea behind measurements will be to take many datapoints (γ, θ_r) and to try to fit such a curve to them. We should note however, that it is quite impossible to cover the whole range $0 \leq \gamma \leq \pi/2$ since for very small γ we encounter total internal reflection. We can see from (6) that this occurs when the argument of $\sin^{-1}$ becomes larger than 1 and the exit angle is no longer real. Solving

$$\cos\left(\sin^{-1}\left(\frac{\sin\gamma}{n}\right) - \alpha\right) = 1 \tag{7}$$

[4]It appears that Greek characters in plots generated by *Mathematica* are not properly recognized by (some versions of) *PostScript*. Therefore, the following conversion may be necessary when reading labels:

$$\begin{aligned}\theta &\leftrightarrow q \\ \alpha &\leftrightarrow a \\ \gamma &\leftrightarrow g\end{aligned}$$

we obtain

$$\gamma_{tir} = \sin^{-1}\left(\sin\alpha + \sqrt{n^2-1}\cos\alpha\right). \tag{8}$$

This angle depends (not surprisingly) on both α and n. A typical value is about 8^o.

2.2 Unknown α

This deflection angle θ_r, and indeed just about any parameter we may think to measure, depends on α as well as n. For $\gamma \gtrsim \pi/4$, the dependence on α is small, but for γ close to γ_{tir} it can become quite large. Figure 3 plots $\partial\theta_r/\partial\alpha$ for $n = 1.0095$ and $\alpha = 0$.

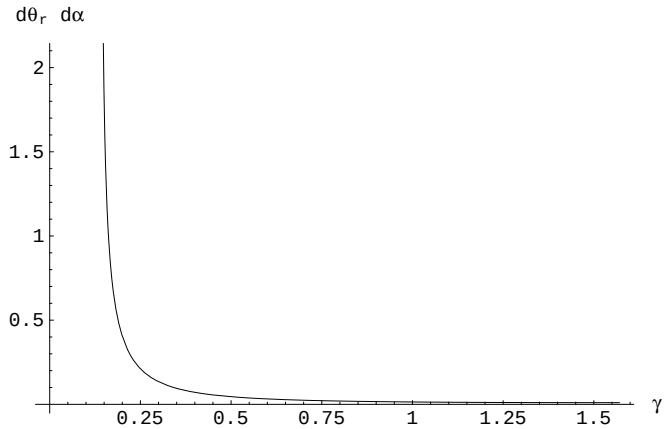

Figure 3: $\dfrac{\partial\theta_r}{\partial\alpha}$ as a function of γ

All this would be fine if we knew or could measure α exactly; but we have not yet found a good method for doing so. (Recall that α is the deviation of the corner angle from $\pi/2$.) Due to the fragility of the aerogel, it has not been possible to do any "mechanical" measurement of the corner angle. The most accurate direct measurements of this angle were done by placing the blocks on a rotating stage (on top of a translational stage) and reading the angles at which a fixed laser beam was parallel to the two smooth sides. This technique gives

$$\begin{aligned}
\alpha_1 &= 0.0 \pm 0.7^o = 0.000 \pm 0.012 \text{ radians}, \\
\alpha_3 &= 0.1 \pm 0.7^o = 0.002 \pm 0.012 \text{ radians}, \\
\alpha_4 &= 0.0 \pm 0.7^o = 0.000 \pm 0.012 \text{ radians},
\end{aligned} \tag{9}$$

for blocks 1, 3, and 4, respectively[5], setting bounds on what the angles may be but

[5]Recall that one block, numbered "2", was broken. The block numbers correspond to their positions in the original container, with the lid on top:

1	3
2	4

not helping too much. There is no reason to assume that all the corner angles are cut to be *exactly* $\pi/2$.

To account for this uncertainty, our curve-fitting of measurements will try to fit both α and n.

2.3 Data collection and error

To measure the deflection angle, the blocks were placed on a precision rotating stage, which in turn was placed on a translational stage. A He-Ne laser beam close to one side of the stage setup was aimed perpendicular to a wall roughly 6 m beyond the stage. The beam first passed through a telescoping lens to attempt to keep it from spreading. Aerogel blocks on the stage could be rotated and brought into and out of the laser beam. A ruler was attached to the wall to measure the horizontal deflection of the beam.

For each set of measurements, we first recorded the distance d between the stage and the projection wall, and the *stage* angle η_0 corresponding to incidence angle $\gamma = \pi/2$. The latter was estimated as in the α measurements, by attempting to align the laser beam parallel to the edge of the aerogel. Note that our measurements had to be calibrated from η_0, not the angle corresponding to "$\gamma = 0$", since measuring the latter via the laser alignment method would have included the uncertainty in α. See Figure 4.

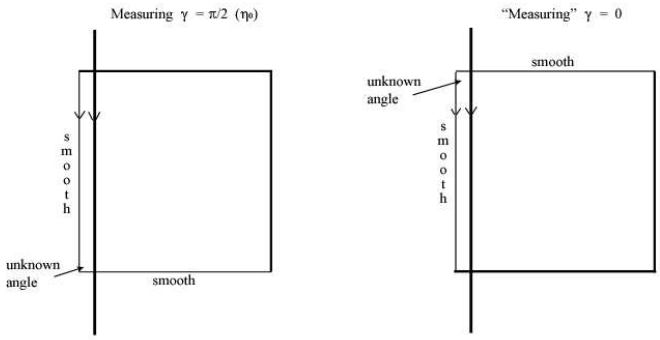

Figure 4: Measuring $\gamma = \pi/2$ vs trying to measure $\gamma = 0$.

Given a horizontal displacement x on the wall, we have

$$\theta_r = \tan^{-1} \frac{x}{d}. \tag{10}$$

Measuring x required measuring the location the centroid of the laser beam on the wall, sometimes a difficult task due to scattering of the beam inside the aerogel and from the surface of its "smooth" sides. The error contribution from x was thus much larger than that from d, and we estimated

$$\delta\theta_r = \frac{\partial\theta_r}{\partial x}\,\delta x = \frac{d}{x^2 + d^2}\,\delta x. \tag{11}$$

The stage angle η could be measured to a precision of ± 0.1 degrees, and η_0 generally to ± 0.3 or ± 0.4 degrees, so the total error in

$$\gamma = \frac{\pi}{2} - \frac{\pi}{180}|\eta - \eta_0| \tag{12}$$

was about $\frac{\pi}{180}(.45) = 0.008$ radians. The error in η_0, however, was systematic across all measurements for a given block (the data analyzed here for each block were all taken at one time, using one η_0), while the error in measuring η was (presumably) randomly distributed. Since the latter was also very small, and many measurements were taken, it has been ignored. The error in η_0 will be dealt with in the following section.

The full set of data can be found in Appendix A. For a given angle, the deflection of the beam was found to depend slightly on *where* it cut the corner of the block; beams very close to the corner were often deflected more than those close to the diagonal (roughly speaking). Therefore, four data points were taken for each value of γ, distinguished by the following labels:

- x: the laser beam cuts through the actual corner of the aerogel, partly inside and partly outside (the centroid of the deflected part of the beam was measured)
- i: the beam is as close as possible to the corner without being split as in x
- m: the beam is midway between the corner and the diagonal
- o: the beam is as close as possible to the diagonal without being split.

The letters initially stood for 'corner', 'in', 'mid', and 'out'. These categories were followed quite strictly for γ around $\pi/4$, but we should note that for extreme values of γ they began to overlap and are less precise descriptions; for $\gamma \approx \pi/2$, an o beam may well be an x beam too. For these extreme values, the labels are used more to designate relative placements of the beam.[6]

One may also note that some data points are not included. Most of the time this was because the beam was too scattered by the aerogel to have a distinguishable, measurable centroid. (For the rest of the datapoints, we measured the error of the centroid location as best as we could.)

2.4 Optimization

Plots of the data for each block can be seen in Figures 5 through 10. Although, as noted above, there is some variation across the location series (x, i, etc.), the points of each individual series generally lie on a distinguishable curve. A very few points, however, seemed to deviate significantly from these trends relative to the size of their

[6] We are beginning to encounter the problem of the smooth sides of the aerogel not being perfectly flat and uniform. More will be said about this in the next section, but we should note that our beam placements and label distinctions are *not* a rigorous method for handling this problem. (One may exist, but is beyond our present scope.) They merely provide a way to include some of this variation in the data.

error bars. Such deviation might have been caused by sharp local irregularities in the aerogel surface, or even experimenter error. So as not to misguide the optimization process, ten of these points, shown in red in Figures 5, 7, and 9, were removed from the data.[7]

For a given n and α, (7) gives the deflection that should be observed. Minimizing

$$\chi^2(n,\alpha) = \sum_i \frac{[\theta_r(\gamma_i, n, \alpha) - \theta_{ri}]^2}{\delta\theta_{ri}^2} \tag{13}$$

should, statistically, give the most likely correct values of n and α for a set of data points (γ_i, θ_{ri}) (assuming α is constant across this data). Moreover, once we find the minimizing values n_0 and α_0, points (n, α) for which

$$\chi^2(n,\alpha) \leq \chi^2(n_0,\alpha_0) + 1 \tag{14}$$

are considered to be within a 1-sigma error of our optimal values. The set of such points generally forms the interior of an ellipse.

Yet we must also consider the error in η_0. To accomodate this, we could include a variable $d\eta_0$ directly in our χ^2 function,

$$\chi^2(n,\alpha,d\eta_0) = \sum_i \frac{[\theta_r(\gamma_i + d\eta_0, n, \alpha) - \theta_{ri}]^2}{\delta\theta_{ri}^2}, \tag{15}$$

and minimize this in the three parameters n, α, and $d\eta_0$ for a given set of data. However, $d\eta_0$ and α seem to be too highly correlated for this to work properly. Overall, the approach that worked best was the following.

For each block, we fixed $d\eta_0$ and minimized $\chi^2(n,\alpha,d\eta_0)$ in n and α for *each* location series (x, i, etc.), obtaining minimum values $\chi_x^2(d\eta_0)$, $\chi_i^2(d\eta_0)$, etc. We then (graphically) minimized

$$\Sigma\chi^2(d\eta_0) = \chi_x^2(d\eta_0) + \chi_i^2(d\eta_0) + \chi_m^2(d\eta_0) + \chi_o^2(d\eta_0), \tag{16}$$

varying $d\eta_0$, to obtain an optimized value $\overline{d\eta_0}$ for the block. Using this value, we reminimized $\chi^2(n,\alpha,\overline{d\eta_0})$ in n and α to obtain optimized values $\overline{n}$ and $\overline{\alpha}$ for each location series, as well as for the combined data ($x+i+m+o$, for a given block).

This approach allows variation in α between the series, as might happen due to a nonplanar or slightly curved aerogel surface, but assumes $d\eta_0$ to be constant for all measurements on a given block. Realistically, surface curvature might also vary $d\eta_0$ from location to location. However, as noted previously, α and $d\eta_0$ tend to be correlated; letting both vary for a given series and minimizing χ^2 in three variables gives (seemingly) wildly inaccurate results and unrealistically large values for both $d\eta_0$ and α. Forcing $d\eta_0$ to be constant across locations largely fixes this problem; since $d\eta_0$ is expected to vary locationally less than α (probably about half as much), it was the variable of choice to do this with.

[7]The main effect of this in the following optimization is to decrease chi^2 values. See Table 6 in Appendix A for a comparison with Table 1.

Block	**Series**	$\overline{\mathbf{n}}$	$\overline{\alpha}$ (radians)	$\overline{\mathbf{d\eta_0}}$ (radians)	**min** χ^2
1	x	1.00970 ± 0.000016	0.0045 ± 0.0005	0.00436	30.46
	i	1.00958 ± 0.000019	0.0024 ± 0.0007	0.00436	29.87
	m	1.00943 ± 0.000047	-0.0154 ± 0.0035	0.00436	18.47
	o	1.00926 ± 0.000037	-0.0173 ± 0.0031	0.00436	31.95
	combined	1.00956 ± 0.000011	-0.0043 ± 0.0004	0.00436	475.61
3	x	1.01048 ± 0.000037	-0.0488 ± 0.0042	-0.02129	16.98
	i	1.00989 ± 0.000048	-0.0452 ± 0.0058	-0.02129	4.63
	m	1.00938 ± 0.000087	-0.0384 ± 0.0057	-0.02129	6.13
	o	1.00956 ± 0.000045	-0.0412 ± 0.0020	-0.02129	22.70
	combined	1.00996 ± 0.000023	-0.0405 ± 0.0016	-0.02129	321.72
4	x	1.00969 ± 0.000025	-0.0060 ± 0.0006	0.00157	5.43
	i	1.00957 ± 0.000021	-0.0069 ± 0.0006	0.00157	17.51
	m	1.00923 ± 0.000032	-0.0039 ± 0.0008	0.00157	11.92
	o	1.00940 ± 0.000055	-0.0076 ± 0.0015	0.00157	10.47
	combined	1.00954 ± 0.000014	-0.0061 ± 0.0003	0.00157	153.001

Table 1: Optimized values of n, α, and $d\eta_0$

The value $\overline{d\eta_0}$ is assumed to be a kind of average optimized value for a given block. It was thus the value used in the combined-data χ^2 optimization for each block.

Resulting values of $\overline{n}$, $\overline{\alpha}$, and $\overline{d\eta_0}$, along with approximate errors for the first two, are shown in Table 1. The errors were computed with the "parabolic approximation", $\frac{\partial^2\chi^2}{\partial y^2} \approx \frac{2}{\sigma_y}$, where $y = n$ or $y = \alpha$. Plots of θ_r using these optimized values are shown alongside the data points in Figures 5, 7, and 9. Figures 6, 8, and 10 show the combined data optimized fits, along with the combined data for each block (plotted with different symbols to help distinguish the series). Finally, Figure 11 plots the 1-sigma ellipses for the χ^2 fits done with $\overline{d\eta_0}$ for each block. Red ellipses correspond to x data, yellow-green to i, green to m, blue to o, and purple to the combined fit. The plot in the bottom left corner superposes the ellipses of the three blocks.

For comparison, Table 7 and Figure 18 in Appendix A show results of χ^2 minimization with $d\eta_0$ always fixed at 0.

2.5 Discussion

We immediately notice several things about the data presented above. The data for block 4 seems excellent, with small error bars and very good fits[8]. Even the combination of the various measurement series in Figure 10 is very tight, perhaps surprisingly so in comparison with the other blocks. Indeed, block 4 seemed to have an exceptionally smooth surface, and to scatter the laser beam the least, allowing for accurate measurements. The fact that the block 4 values of $\overline{\alpha}$ and $\overline{d\eta_0}$ are small and

[8]Except for the three removed points. But, as shown in Table 6, removing these three points really does not affect much at all in terms of optimization.

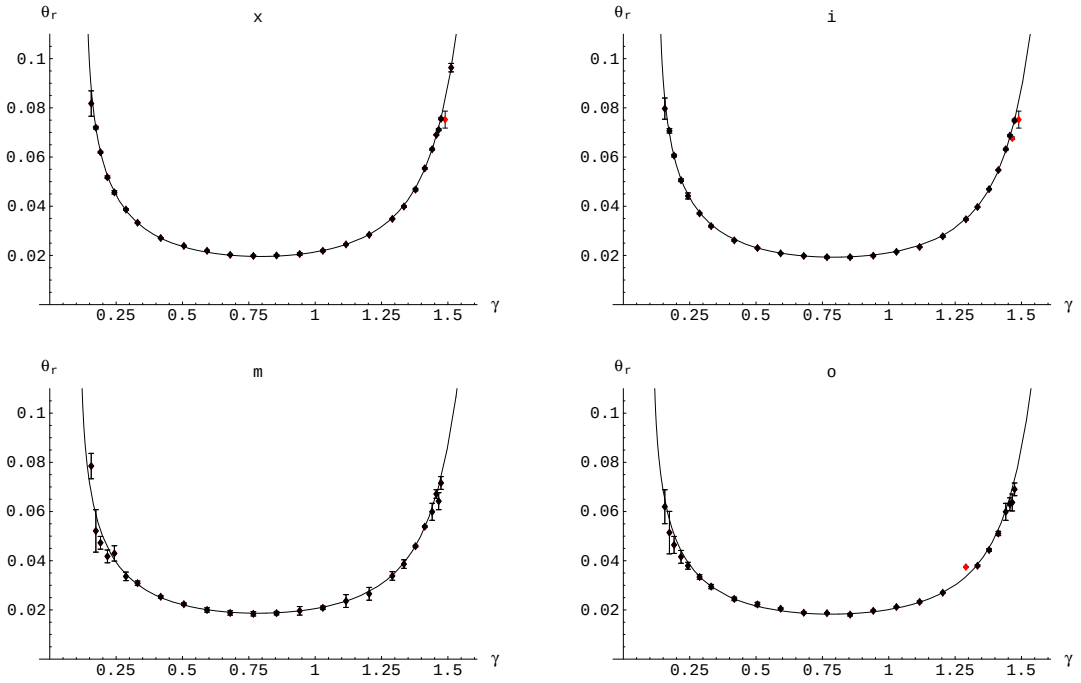

Figure 5: Data for Block 1 (all angles in radians)

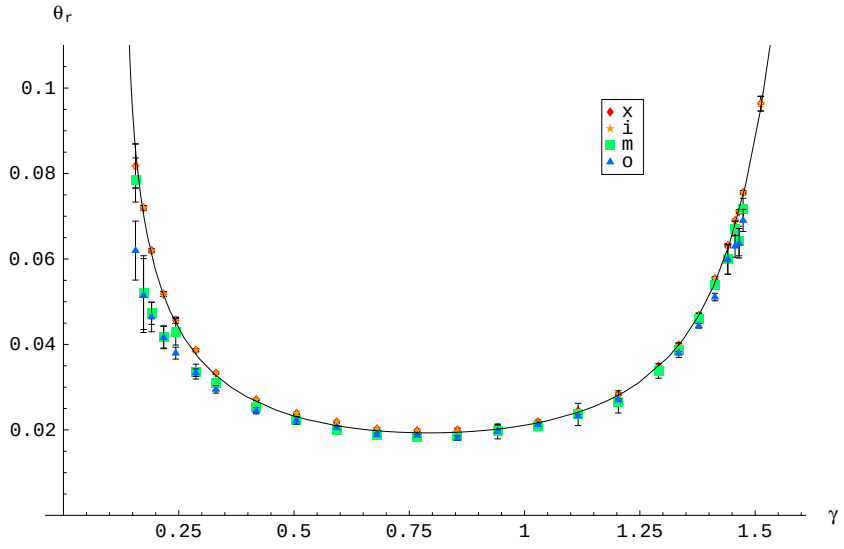

Figure 6: Combined data for Block 1

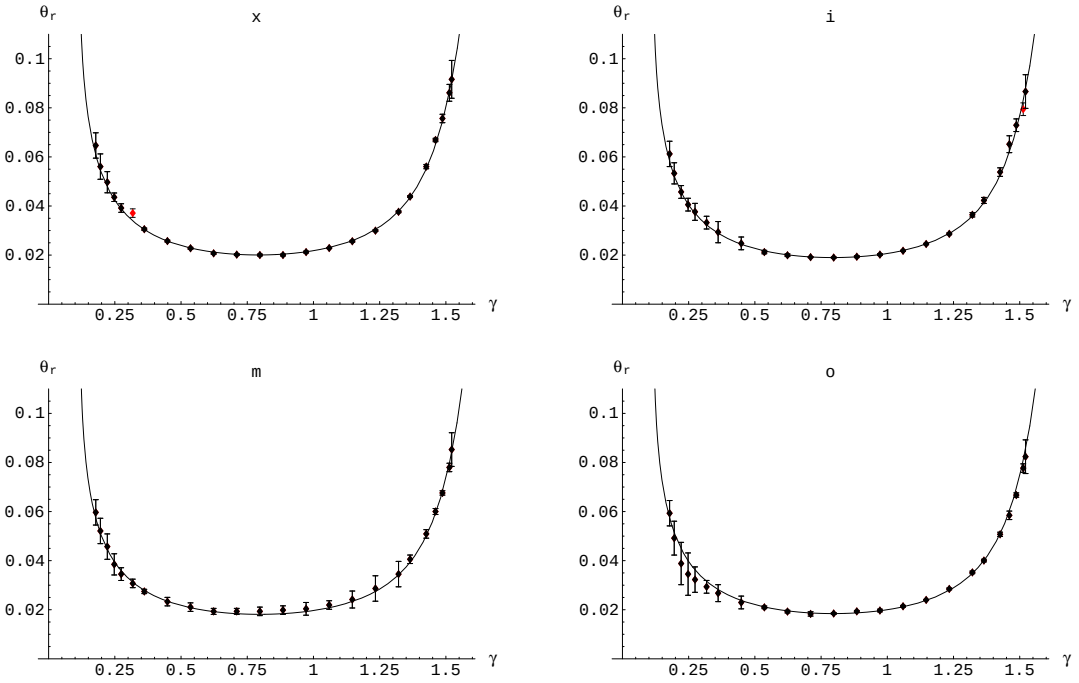

Figure 7: Data for Block 3 (all angles in radians)

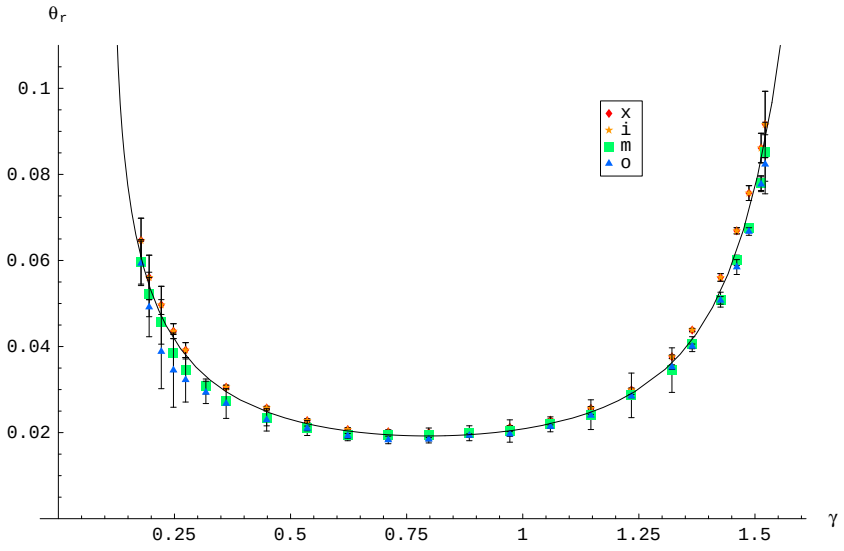

Figure 8: Combined data for Block 3

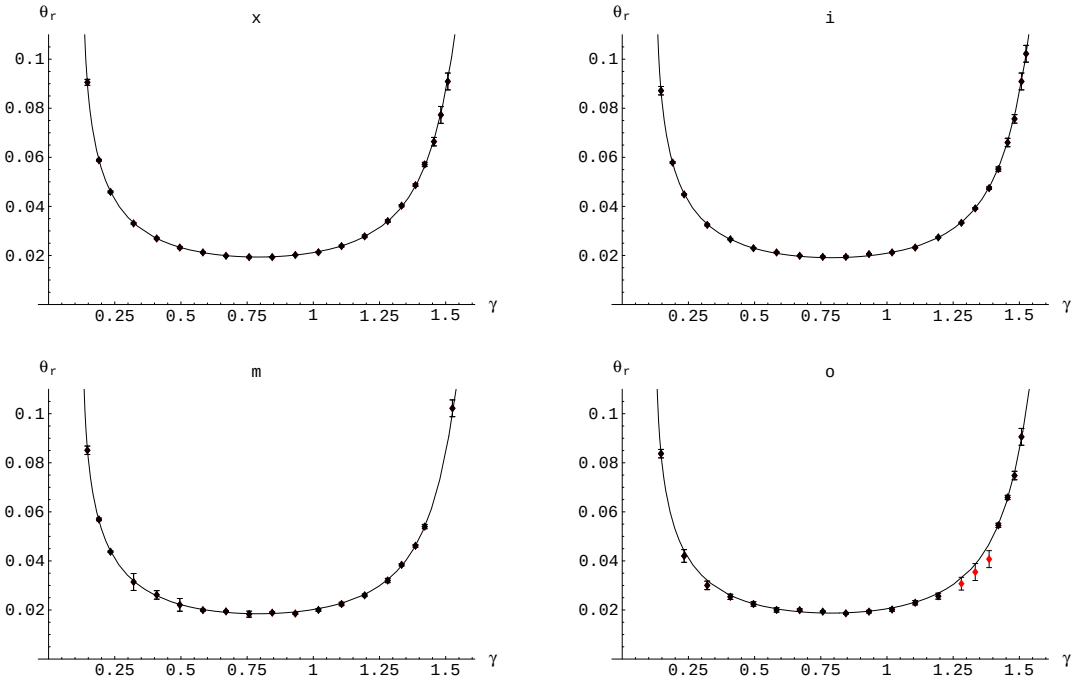

Figure 9: Data for Block 4 (all angles in radians)

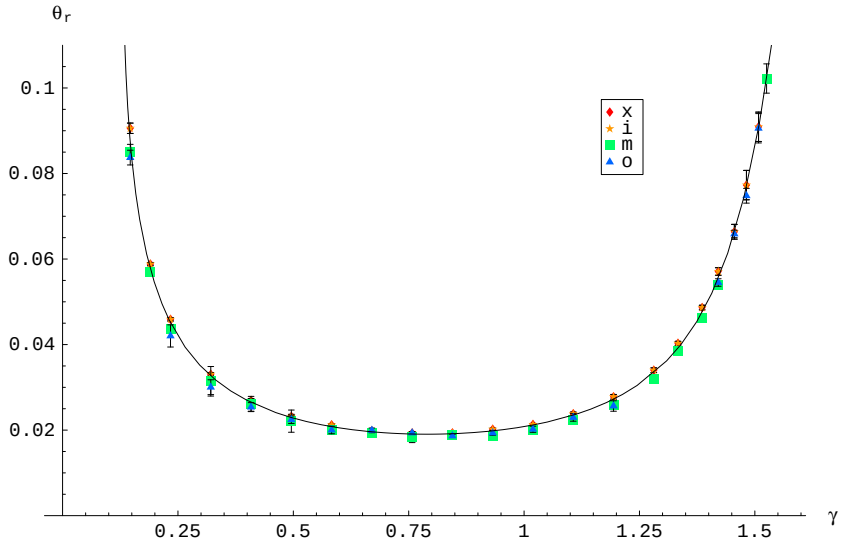

Figure 10: Combined data for Block 4

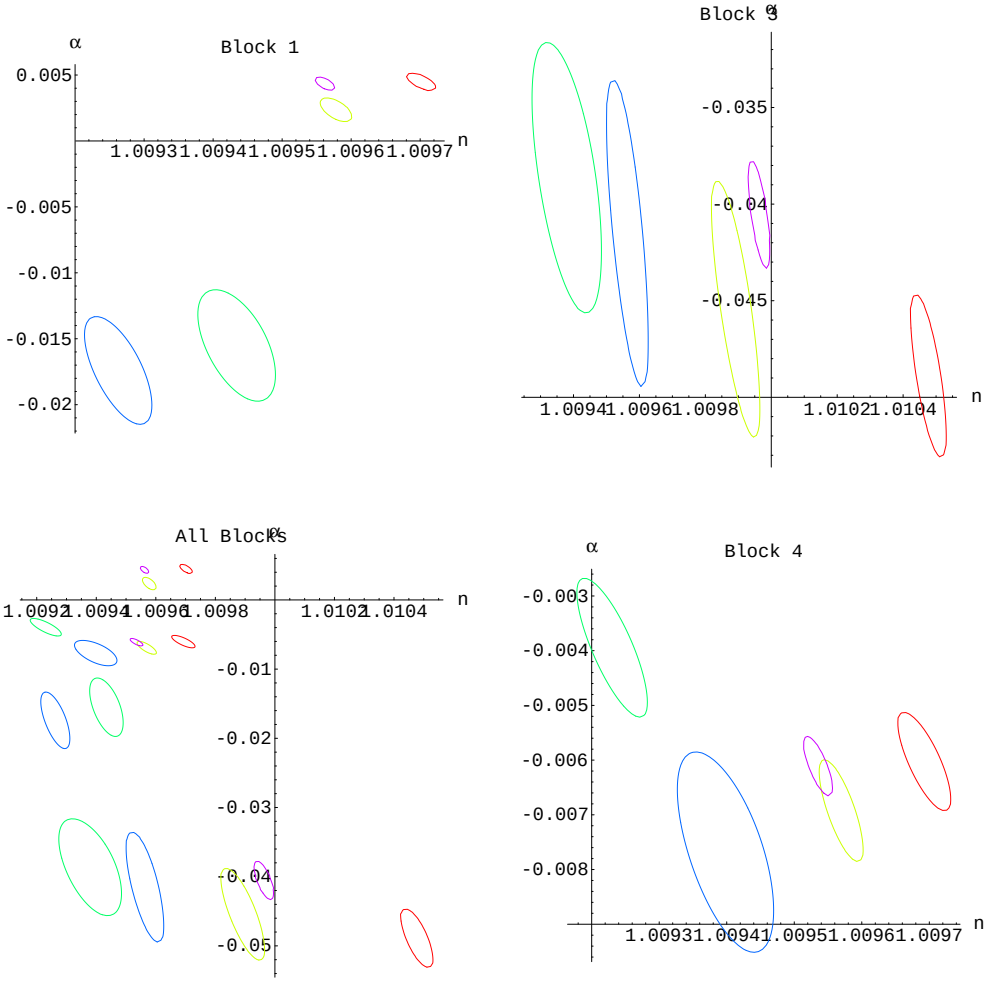

Figure 11: 1-sigma error bounds

(in the case of $\overline{\alpha}$) do not vary too much between the location series, and the tightness of the data in Figure 10, show that the surface of block 4 was probably very flat as well as optically smooth.

Block 1 also provided decent data, though it was not as good as block 4. Experimentally, its surface was not quite as smooth. Nevertheless, the optimized curves in Figure 5 do agree with the data very well, except perhaps for some cloudy zones in the m and o series for extreme values of γ. The combined plot shows some variation among the series; m and o seemed consistently to favor less refraction than x and i, a pattern that also appears for block 3. This caused the lower values of $\overline{n}$ in Table 1. Block 1 also gave a higher $\overline{d\eta_0}$ and more variation in $\overline{\alpha}$, perhaps corresponding to some slight (outward) curvature in the aerogel surface.

Recall that (essentially for all three blocks) we had roughly measured $\alpha = 0 \pm 0.012$ radians and knew $d\eta_0 = 0 \pm 0.007$ radians (0.4 degrees). For block 1, the value of $\overline{d\eta_0}$ is acceptable, but the values of $\overline{\alpha}$ are pushing this limit. For block 3, the optimized values of both are far beyond admissible error. It is also (visibly) clear that the optimized curves do not fit the data of block 3 very well. Evidently, the optimization process did not entirely work in this case. We should note, however, that block 3 had by far the roughest surface of the three blocks, and, as indicated by the error bars in Figure 7, its data contained significantly more measurement error. Perhaps this was the cause of the optimization difficulties.

The error ellipses in Figure 11 reinforce the above observations. For blocks 1 and 4, particularly for the x, i, and combined locations, the ellipses are very small. For block 3, on the other hand, they are much larger. They are spread out over a wider range, centering around values of $\overline{n}$ very different from those of blocks 1 and 4 (which are very similar).

Looking at Figure 11, however, we may notice a different problem: none of the error ellipses for a given block actually overlap! (This problem can also be seen from the errors in Table 1.) A spread in the α direction might be acceptable, but the spread in n, with relatively small error, is not. Evidently, the error somewhere in our methods is significantly larger than what we had estimated. And perhaps even more striking is the general pattern of spread that the ellipses for each block seem to follow (with some variation). We marked earlier that m and o seem to show less deflection than x and i; this is the result in terms of $\overline{n}$ and $\overline{\alpha}$ (again, we could have also seen this from Table 1, but the visual version is more vivid). It seems that there is some parameter, varying with location, that we have not accounted for. This may not have too much to do with some overall surface curvature, because we *did* let α vary.[9] More likely a suspect is some effect of the interior of the aerogel on light passing through it. It *is* a significantly dispersive medium, and m and o beams would pass through increasingly more of it than x and i beams. But just what this effect might be has not been determined; the present calculations are currently the best we have.[10]

[9] As we mentioned at the end of the last section, letting $d\eta_0$ vary with location as well only worsens the situation.

[10] Also compare Figure 18: the same situation appears. The spread, and the characteristic pattern of the ellipses for a given block, is not a side effect of our slightly unorthodox η_0 optimization. There *is* some inherent factor influencing the data.

If passage through the interior of the block is somehow affecting deflection angle, x and i measurements should be the most dependable. But, because the m and o error bars are generally larger (due to increased passage through the dispersive aerogel interior), the combined location fits actually tend to favor the x and i data. This can easily be seen from the combined fit curves, or the location of the purple ellipses in Figure 11. Given the high probable error in block 3 data and optimization (as described above), and the fact that Blocks 1 and 4 agree extremely well on x, i, and combined values of $\overline{n}$, it may be best to disregard the former. Then, using the combined fits for blocks 1 and 4, we can say the most likely value of the real n is 1.00955. What is the error on this? χ^2 fitting would suggest ± 0.00002 as a generous error bound; but given the preceding discussion this is evidently too small. An error of ± 0.00015 is more reasonable. This covers all the x and i values for blocks 1 and 4, as well as the m value for block 1 and the o for block 4. As our best estimate from these measurements, we may then quote

$$n = 1.00955 \pm 0.00015. \tag{17}$$

Notice, incidentally, that the deflection curve corresponding to $n = 1.00955$, $\alpha = -0.008$, and $d\eta_0 = -0.003$ fits the x and i measurements of block 3 quite well, better even than the automatically optimized curve. The curve is plotted together with block 3 data in Figure 12. To this extent, block 3 confirms our choice of n for the aerogel.[11]

3 Method 2: Interferometry

The second method if determining the aerogel's index of refraction used interferometry. The wavelength of light in the aerogel is reduced by a factor of n; hence laser light of wavelength λ_0 has wavelength λ_0/n inside the aerogel. Placing a block of aerogel diagonally in a beam (as in the refraction method) and moving it perpendicularly to the beam, it is possible to continuously vary the length of the beam path in the aerogel. By using an interferometer to count the number of wavelengths gained (or lost) as the aerogel was moved a certain distance into (or out of) a laser beam, we hoped to obrtain accurate estimates of n.

The interferometer we used is shown in Figure 13. A laser beam (coming from the left) was split into two beams, one of which travelled through aerogel and the other only through air. The beams were then recombined (by using adjustable mirrors to properly align them), and the recombined beam was magnified and projected onto a screen. When the aerogel surface was sufficiently smooth, a discernable fringe pattern appeared on the screen, each fringe corresponding to a 1-wavelength difference between the split beams.

[11] The "fitting" was done visually, since automatic optimization evidently does not perform well for block 3 measurements and their error. This new curve hits slightly low of the measured x and i deflection for central values of γ, and also misses a few extreme m and o data points with small error bars, causing χ^2 to rise to 668.33: about double its minimized value, but not too bad. Notice (Table 7) that this is almost exactly the χ^2 value obtained by holding η_0 fixed at 0.

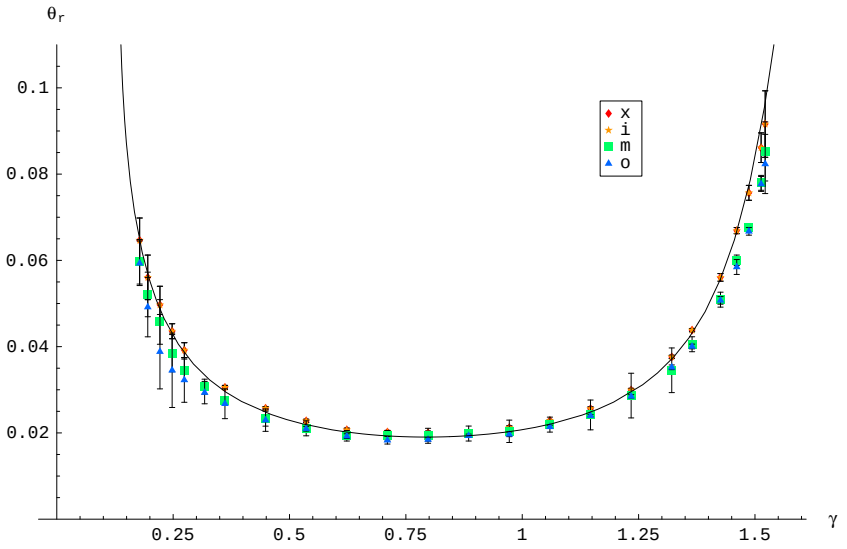

Figure 12: Block 3 data, with a new fit ($n = 1.00955$, $\alpha = -0.008$, $d\eta_0 = -0.003$)

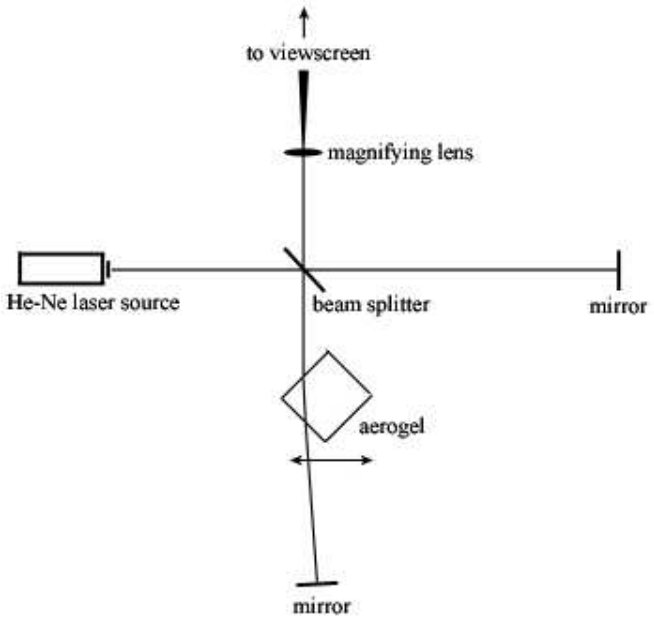

Figure 13: The interferometer

3.1 Preliminary calculations

Assuming a perfectly square block of aerogel mounted so that the laser beam is incident at 45 degrees, and assuming that any refraction is negligible (such a setup is shown in Figure 14, we may estimate the wavelength shift upon moving the block a distance Δd into or out of the beam.

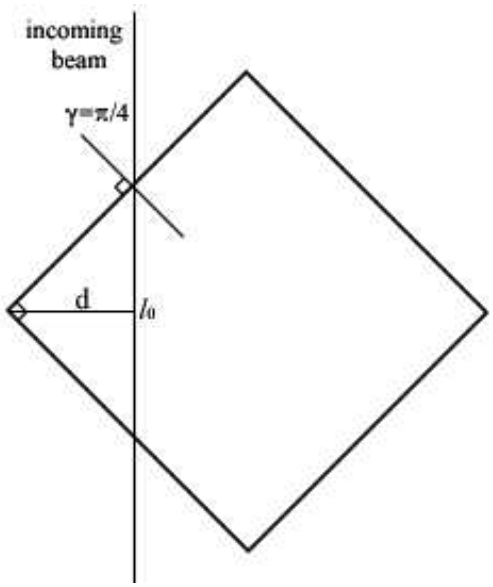

Figure 14: A naive view of wavelength shift

If the block is a perpendicular distance d inside the beam, the beam path length inside the aerogel is $l_0 = 2d$. Since the wavelength in the aerogel is λ_0/n, the beam thus travels

$$q_g = \frac{2d}{\lambda_0/n} = \frac{2dn}{\lambda_0} \tag{18}$$

wavelengths in the aerogel per perpendicular distance d. But the beam also "looses" the wavelengths it would have otherwise traveled in air. In this setup, this is also a distance $2d$, corresponding to

$$q_a = \frac{2d}{\lambda_0} \tag{19}$$

wavelengths.[12] Therefore, the total *gain* in wavelengths as the block is pushed a distance d into the beam is

$$q = q_g - q_a = \frac{2d}{\lambda_0}(n-1) \tag{20}$$

. We should remember, however, that in our interferometer setup (Figure 13) the beam traverses the block twice, one coming from the beam splitter, and again after

[12] Again, we assume the index of refraction of air is exactly 1. Comments similar to those of Footnote 3 apply.

being reflected back to the beam splitter. So in fact we have for our final estimate:

$$q = \frac{4d}{\lambda_0}(n-1) \tag{21}$$

and

$$n = \frac{q\lambda_0}{2d} + 1. \tag{22}$$

Since q is proportional to d in Equation 21, we can always write Δq and Δd in place of q and d.

Using a Helium-Neon laser with $\lambda_0 = 632.8$ nm, and assuming the index of refraction is roughly 1.0096, we see that we would have to move the block a distance of

$$d = \frac{(.6328)}{4(.0096)} = 16.5\ \mu\text{m} \tag{23}$$

to effect a 1-wavelength shift (*i.e.* the passing of one interference fringe).

3.2 More thorough calculations

The above calculations, however, are of course not quite correct. They overlook the slight refraction of the beam, an uncertainty (α) in the corner angle, and an uncertainty in the angle of incidence γ. They are simple and very useful for estimating the effects of moving the block; but if we are to accurately calculate n we need to know about these other factors.

Figure 15 shows a more realistic view of the situation, using the same notation that was used in the refraction calculations. The real beam path is in black, following the incident beam, x_1, x_2, and the black exiting beam. The purple angles correspond to the triangle formed by the real beam path and the corner of the block. The path the beam *would* have taken, had d been 0, is shown in blue and green, following the incident beam, l_1, l_{2p}, and the green exiting beam. Note that we still include a deflection of θ_r in this path; in a sense it corresponds to $d = 0^+$. We want to calculate the wavelengths gained by passage through the aerogel, a path length x_1+x_2, minus the wavelengths that would have been traveled in air. The latter distance is $l_1 + l_{2p} - l_{2m}$, where we must take into account the difference in path length caused by "shifting" of the exit beam on the mirror surface. (The mirror is always aligned perpendicular to the exiting beam, to reflect it back along the same path.)

The easiest quantity to calculate is l_1:

$$l_1 = d\tan\gamma. \tag{24}$$

To find x_1, we first get $y_1 = \frac{d}{\cos\gamma}$ and then use the law of sines:

$$\begin{aligned} x_1 &= y_1 \frac{\sin\gamma}{\sin(\pi/2 + \theta_1 - \gamma)} \\ &= d\frac{\tan\gamma}{\cos(\gamma - \theta_1)} \end{aligned} \tag{25}$$

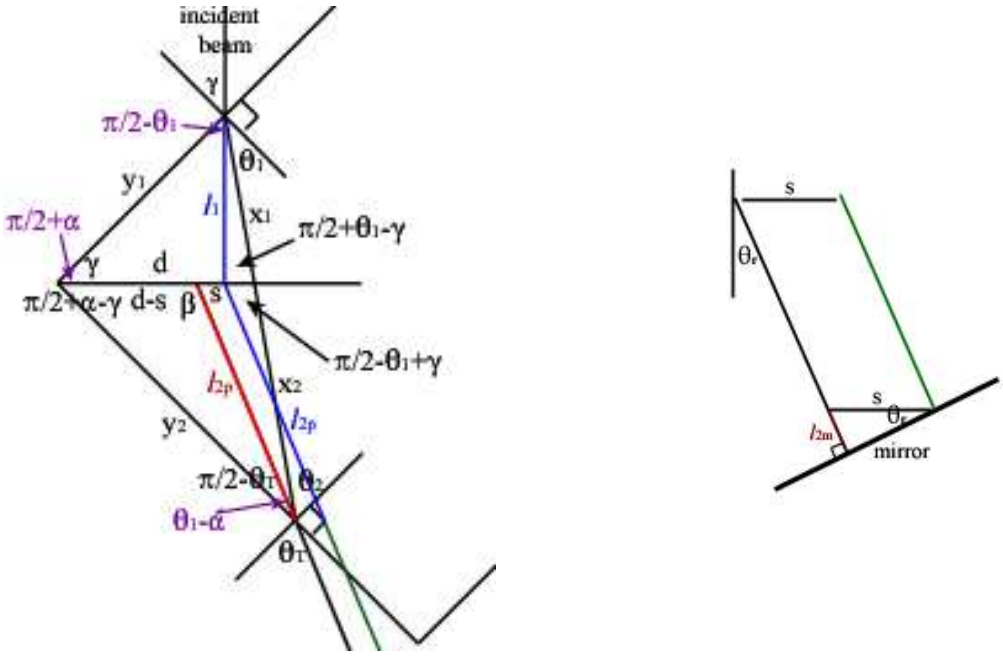

Figure 15: A better view of wavelength shift

We may also use the law of sines on the large (purple-labeled) triangle to find y_2,

$$\begin{aligned} y_2 &= y_1 \frac{\sin(\pi/2-\theta_1)}{\sin(\theta_1-\alpha)} \\ &= d\frac{\cos\theta_1}{\sin(\theta_1-\alpha)\cos\gamma}, \end{aligned}$$

and again to obtain x_2,

$$\begin{aligned} x_2 &= y_2 \frac{\sin(\pi/2+\alpha-\gamma)}{\sin(\pi/2-\theta_1+\gamma)} \\ &= d\frac{\cos(\gamma-\alpha)\cos\theta_1}{\sin(\theta_1-\alpha)\cos(\gamma-\theta_1)\cos\gamma}. \end{aligned} \tag{26}$$

The same approach works to get l_{2p}. Since $\beta = \pi - (\pi/2+\alpha-\gamma) - (\pi/2-\theta_T) = \gamma - \alpha + \theta_T$, we have

$$\begin{aligned} l_{2p} &= y_2 \frac{\sin(\pi/2+\alpha-\gamma)}{\sin(\gamma-\alpha+\theta_T)} \\ &= d\frac{\cos(\gamma-\alpha)\cos\theta_1}{\sin(\gamma-\alpha+\theta_T)\sin(\theta_1-\alpha)\cos\gamma}. \end{aligned} \tag{27}$$

(Here we have solved for the *red* l_{2p} in Figure 15, which is the same length as the the *blue* l_{2p}, the length that would have been traveled in air.) The path change at the

mirror is a function of the total deflection angle, $\theta_r = \gamma - \alpha + \theta_T - \pi/2$ (by (7)), and the shift perpendicular to the incident beam, s. We have

$$\begin{aligned} d - s &= y_2 \frac{\sin(\pi/2 - \theta_T)}{\sin(\gamma - \alpha + \theta_T)} \\ \Rightarrow \quad s &= -d \left(\frac{\cos\theta_1 \cos\theta_T}{\sin(\gamma - \alpha + \theta_T)\sin(\theta_1 - \alpha)\cos\gamma} - 1 \right), \end{aligned}$$

and

$$\begin{aligned} l_{2m} &= s \sin\theta_r \\ &= -s\cos(\gamma - \alpha + \theta_T) \\ &= d \left(\frac{\cos\theta_1 \cos\theta_T}{\tan(\gamma - \alpha + \theta_T)\sin(\theta_1 - \alpha)\cos\gamma} - \cos(\gamma - \alpha + \theta_T) \right). \end{aligned} \tag{28}$$

Using Equations 4 and 6 to substitute for θ_1 and θ_T, we can express x_1, x_2, l_1, l_{2p}, and l_{2m} entirely in terms of α, γ, and n. The substitutions are not shown here explicitly due to the complexity of the expressions and the little insight they offer directly.

Taking into account, as before, that the beam traverses the block *twice*, the total number of wavelengths gained when the block is a perpendicular distance d inside the beam is

$$q = \frac{2nl_0}{\lambda_0} - \frac{2(l_1 + l_{2p} + l_{2m})}{\lambda_0} = \frac{2d}{\lambda_0} \left(n\frac{l_0}{d} - \frac{l_1 + l_{2p} + l_{2m}}{d} \right), \tag{29}$$

where we have written l_0 for $x_1 + x_2$. Notice that q is still directly proportional to d, allowing us to replace q and d by Δq and Δd where we like.

The key problem now is to solve (29) for n. It is clear, however, that there is no simple way to do this. At best it seems that we could reduce it to some high-degree polynomial equation in n; but from there the problem would be intractable. We can, however, approximate the right hand side as a Taylor series in the very small quantity $n - 1$. Letting

$$L(n) = \frac{nl_0}{d} - \frac{l_1 + l_{2p} + l_{2m}}{d} \tag{30}$$

we can say

$$\frac{q\lambda_0}{2d} = L(1) + L'(1)(n-1) + \frac{1}{2}L''(1)(n-1)^2 + O((n-1)^3) \tag{31}$$

(we shall justify keeping second order terms later), which becomes

$$\frac{1}{2}(n-1)^2 + \frac{L'(1)}{L''(1)}(n-1) + \frac{1}{L''(1)} \left(L(1) - \frac{q\lambda_0}{2d} \right) \approx 0 \tag{32}$$

$$\Rightarrow \qquad n \approx -\frac{L'(1)}{L''(1)} \pm \sqrt{\left(\frac{L'(1)}{L''(1)} \right)^2 - \frac{2}{L''(1)} \left(L(1) - \frac{q\lambda_0}{2d} \right)} + 1. \tag{33}$$

Evaluating derivatives and simplifying, we find[13]

$$L(1) = 0 \tag{34}$$

$$L'(1) = \frac{\cos\alpha}{\sin(\gamma-\alpha)\cos\gamma} \tag{35}$$

$$\begin{aligned} L''(1) &= \frac{1}{16\sin^3(\gamma-\alpha)\cos^3\gamma}\left[3\cos 3\alpha - 5\cos\alpha + \cos(4\gamma-\alpha) + \cos(4\gamma-3\alpha) - 24\cos(2\gamma-\alpha)\right. \\ &\quad \left. -8\cos(2\gamma-3\alpha) - 16\cos(2\gamma+\alpha)\right] \end{aligned} \tag{36}$$

$$L'''(1) = \text{a similar but longer expression.} \tag{37}$$

Now, we can drop higher order terms from expression (31) only if the higher order L derivatives are sufficiently small for $n = 1$. Around $\alpha \approx 0$ and $\gamma \approx \pi/4$, we have

$$L'(1) \approx 2, \qquad L''(1) \approx -2, \qquad L'''(1) \approx -114. \tag{38}$$

For an index $n \approx 1.01$, a wavelength $\lambda_0 \approx 633$ nm, and a distance $d = 1650$ μm, we get

$$\frac{2d}{\lambda_0}(L(1)+L'(1)(n-1))2 \approx 104.265, \quad \frac{2d}{\lambda_0}\frac{1}{2}L''(1)(n-1)^2 \approx -0.521, \quad \frac{2d}{\lambda_0}\frac{1}{6}L'''(1)(n-1)^3 \approx -0.099 \tag{39}$$

as well as the exact value

$$\frac{2d}{\lambda_0}L(1.01) \approx 103.644. \tag{40}$$

Without calculating them, we thus see that other higher-order terms (above third order) do not contribute more than 0.001. Experimentally, the error in counting 100 passing fringes was usually about one fringe, and at best about half a fringe. We thus see that we must keep the second order term in the expansion (which is of the same magnitude as this error), but may, to a reasonable approximation, drop third order and higher.

Now, $-L'(1)/L''(1) = 1$ is positive for $\alpha = 0$ and $\gamma = \pi/4$, and the square root in (33) is a little bit less than $-L'(1)/L''(1)$, so it appears that we should take the negative root in Equation 33. However, for some nearby values of α and γ, $L''(1)$ actually grows to 0 and then becomes positive ($L'(1)$ remains positive throughout the experimental range). Thus we must have

$$n = \begin{cases} -\dfrac{L'(1)}{L''(1)} - \sqrt{\left(\dfrac{L'(1)}{L''(1)}\right)^2 + \dfrac{q\lambda_0}{L''(1)d}} + 1, & L'(1)(\gamma,\alpha) < 0 \\ -\dfrac{L'(1)}{L''(1)} + \sqrt{\left(\dfrac{L'(1)}{L''(1)}\right)^2 + \dfrac{q\lambda_0}{L''(1)d}} + 1, & L'(1)(\gamma,\alpha) > 0 \end{cases} \tag{41}$$

As shown in Figure 16, this function is continuous, and its limit at $L''(1) = 0$ is well-defined. Indeed, the function is differentiable (in d, q, γ, and α) throughout the entire range of interest.[14]

[13]The form of $L''(1)$ is slightly strange because the expression was simplified by *Mathematica* rather than by hand.

[14]Strictly speaking, the function defined by (41) when $L'(1) \neq 0$ and the limit of either of the functions in (41) when $L'(1) = 0$ is differentiable. We do not prove this rigorously here.

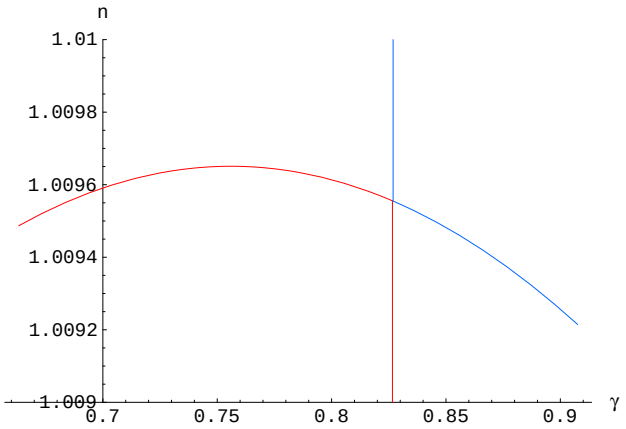

Figure 16: Plot of $n(q = 100, d = 1650\mu\text{m}, \lambda_0 = .6328\mu\text{m}, \gamma, \alpha = 0)$ around its singularity. The case $L''(1) < 0$ is in red, and $L''(1) > 0$ in blue.

3.2.1 Error propagation

As for the refraction method, we estimate the error in measuring n by

$$\delta n = \sqrt{\left(\frac{\partial n}{\partial d}\delta d\right)^2 + \left(\frac{\partial n}{\partial q}\delta q\right)^2 + \left(\frac{\partial n}{\partial \alpha}\delta \alpha\right)^2 + \left(\frac{\partial n}{\partial \gamma}\delta \gamma\right)^2}. \tag{42}$$

We assume that λ_0 is known precisely; for Helium-Neon lasers, the value of 632.8 nm is sufficiently accurate. The derivatives are rather complicated expressions and there seems no need to write them out explicitly.

Note that (41) was specifically derived to measure n as a function of varying d and q (or the one parameter q/d); α and γ are assumed fixed for each set of measurements. Generally speaking, we could not use the same equation to calculate n from a number Δq of passing fringes as γ varies. The block would be moved in a fundamentally different way. We assume, however, that the partial derivatives in α and γ are still good approximations for the error. (This is akin, for example, to the difference between rotation about a point on the perimeter of a wheel and rotation about its center. In certain cases, and for infinitesimal rotations, the two may be considered approximately the same. . . .)

3.3 Data collection

The full data set appears in Appendix B.

The interferometer itself was described at the beginning of Section 3, and is shown in Figure 13. Its two arms were each roughly 25 cm long. As for the refraction method, the aerogel was mounted on a double stage, a rotating stage on top of a precision translational stage. The accuracy of the former was about 0.2 degrees, and of the latter about 1 micron.[15] At the beginning of each set of measurements on a block,

[15]These are *not* the same stages used in the refraction measurements; the more precise rotating

we measured the stage angle η_0 corresponding to $\gamma = \pi/2$ (see Figure 4 and the surrounding discussion), then turned the aerogel to $\gamma \approx \pi/4$. The error in measuring η_0 was about .4 degrees, and that in setting/measuring the final γ angle about .2 degrees (the error of the stage). Altogether, this resulted in an error of about

$$\delta\gamma \approx \sqrt{0.4^2 + 0.2^2} \approx 0.45 \text{ degrees.} \tag{43}$$

The values of α used in refraction, given in (9), came from a combination of measurements done both here and in refraction. They will be used here as well, along with the optimized values of $\overline{\alpha}$ given by the refraction method, as described in the next section.

Once a block of aerogel was at $\gamma \approx \pi/4$, we positioned it vertically and horizontally (perpendicular to the beam) until transmission was good enough to form a fringe pattern. (This also involved adjusting the mirror of interferomoter's aerogel arm to keep the two split beams aligned.) An initial horizontal position was read, and we began slowly changing this horizontal position. After a certian number q of fringes passed, we read the final horizontal position. Then we either kept going, taking another data point, or repositioned the block to another clear transmission spot before moving on.

All positions measured correspond roughly to the i (or i to m) regions of the block as described for refraction: we generally tried to stay near the corner of the blocks. This minimized dispersion within the aerogel, giving clearer transmission and better fringes. (Recall that this was also the region of cleanest measurements in the refraction method.)

The error in the horizontal distance moved, d, came entirely from the precision of the stage, and so is about $\sqrt{1^2 + 1^2} = 1.4$ microns for all measurements. The error in the number of fringes q was estimated for each measurement. Since we were using a laser beam of small but finite diameter, different parts of which were going through different thicknesses of aerogel, and since the surface of the blocks was never perfectly smooth, we never obtained a completely perfect fringe pattern. Indeed, the fringe pattern itself often changed and shifted as the surface of the aerogel varied over the distance moved. We generally counted between 10 and 100 fringes, trying to count as many as possible without having the fringe pattern change; but sometimes staying within a constant pattern was just not feasible. The estimated error in fringes that might have been miscounted is reported.

3.4 Analysis and Discussion

The values of n calculated from the data are shown in Figure 17. Data from block 1 is in red, block 3 in green, and block 4 in blue. Calculations for all blocks used $\alpha = 0$. The error bars correspond to error from q, d, and γ, but not α. Errors from q and d should be randomly distributed for each measurement, and including them in the form of general error bars is quite appropriate. As explained in the preceding section, error from γ is essentially systematic over each set of measurements. But

stage used there was too large to combine with the precise translational stage used here.

the measurements for each block come from three or four different sets. And the contribution from γ error is also almost insignificantly small. (For typical values $q = 100$ and $d = 1650$ μm, and the entire range $-2^\circ \leq \alpha \leq 2^\circ$ and $43^\circ \leq \gamma \leq 47^\circ$, $\frac{\partial n}{\partial \gamma}(.45^\circ)$ never gets bigger than 0.000025.) The γ error was thus included in the error bars as well.

The error from α, however, is (essentially) systematic for each block, depending only on the block's *real* value of α, and so was kept separate. Across all our measurements, we have

$$-0.000123 < \frac{\partial n}{\partial \alpha}(.7^\circ) < -0.000092, \tag{44}$$

showing the maximum possible error from α given by (9). (We thus see that $\partial n/\partial \alpha$ remains quite constant across our range of paramameters.)

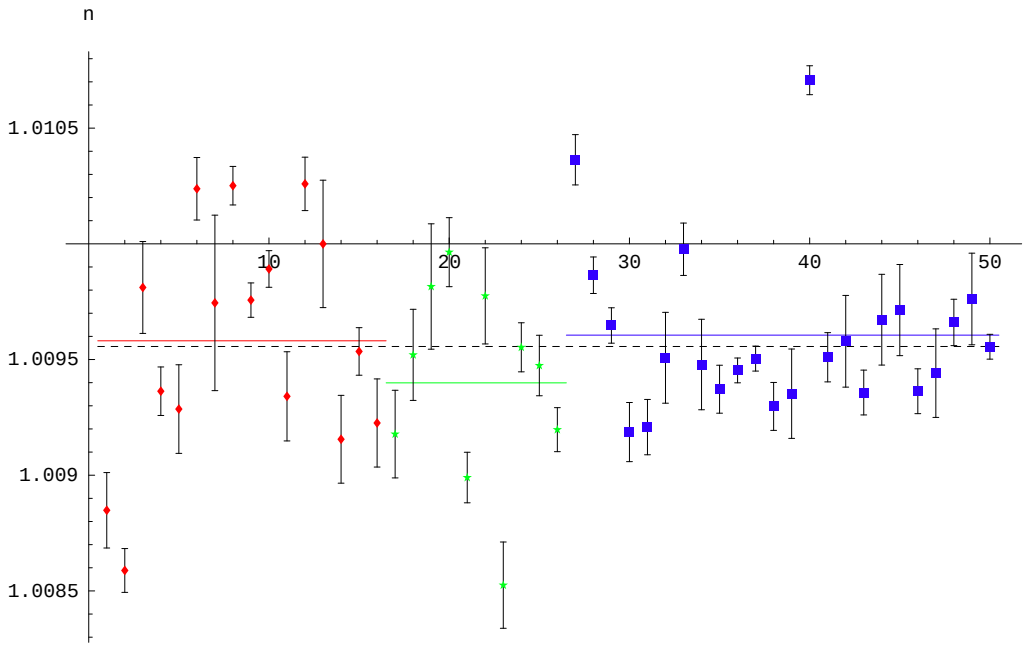

Figure 17: Calculated values of n; numbering on the horizontal axis corresponds to data points

Unfortunately, we see in Figure 17 a spread of n values much larger than the estimated error bars. Since measurements were taken over ranges of only 1 or 2 millimeters, it is highly probable that this spread is due mostly to local surface irregularities of the aerogel. A surface 'bump' of a few microns could throw off measurements substantially. Indeed, we see that the data points for block 4, which had by far the smoothest surface, are tighter than for blocks 1 and 2. (But still there are two very deviant block 4 points.) Generally, finding the most likely value of the index would involve minimizing χ^2 as we did for the refraction method; in this case, the result

would be

$$\overline{n}_{\chi^2} = \frac{\sum \frac{n_i}{\delta n_i^2}}{\sum \frac{1}{\delta n_i^2}} \tag{45}$$

(a weighted average). However, assuming the spread does indeed arise from local irregularities, it seems best to ignore error bars (or assume all δn_i are equal). The above expression then simplifies to the ordinary mean value of n,

$$\overline{n} = \frac{\sum n_i}{N}. \tag{46}$$

The error in *oln* is then best estimated by the standard deviation of the data points. Table 2 shows mean values and standard deviations for each block separately and for the combined set of data. The χ^2 minimized value is included for comparison. The solid fit lines in Figure 17 also correspond to these mean values.

Block	$\overline{\mathbf{n}}$	$\overline{\mathbf{n}_{\chi^2}}$	$\sigma_{\mathbf{n}}$
1	1.00958	1.00965	0.00050
3	1.00940	1.00935	0.00043
4	1.00961	1.00966	0.00035
combined	1.00956	1.00962	0.00042

Table 2: Mean values and standard deviations of n

Our final task is to use this data to report a single value of n. Assuming real values of α are 'randomly' distributed among the three blocks, a simple solution would be to use the combined value,

$$n_c = 1.00956 \pm 0.00042. \tag{47}$$

This does not weigh the data from each block equally. But the number of measurements taken for each block correspond roughly to the clarity of transmission and the quality of fringes produced by that block, so this would not be an inappropriate weighted average. A better solution, however, is to take an actual (χ^2) weighted average of values from the three blocks, considering them as separate measurements of n. The standard deviations *should* indicate precisely the smoothness of the surfaces; assuming randomly distributed α and its error contibution (44), we estimate the total error for the blocks as

$$\begin{aligned} \sigma_1 &\approx \sqrt{0.00050^2 + 0.0001^2} = 0.00051 \\ \sigma_3 &\approx \sqrt{0.00043^2 + 0.0001^2} = 0.00045 \\ \sigma_4 &\approx \sqrt{0.00035^2 + 0.0001^2} = 0.00036. \end{aligned} \tag{48}$$

Then our final estimate for n would be

$$n = \frac{\frac{\overline{n}_1}{\sigma_1^2} + \frac{\overline{n}_3}{\sigma_3^2} + \frac{\overline{n}_4}{\sigma_4^2}}{\frac{1}{\sigma_1^2} + \frac{1}{\sigma_3^2} + \frac{1}{\sigma_4^2}} = 1.00954, \tag{49}$$

and

$$\delta n = \frac{1}{\frac{1}{\sigma_1^2} + \frac{1}{\sigma_3^2} + \frac{1}{\sigma_4^2}} = 0.00025, \tag{50}$$

$$\Rightarrow \quad n = 1.00954 \pm 0.00025. \tag{51}$$

Except for the smaller estimated error, this is not too different from n_c; it is the best value we can report at the moment. The dashed line in Figure 17 corresponds to this value. Note that the error is more than large enough to encompass the mean values for each of the blocks.

3.4.1 A comment on α and block cutting

Since the four (initial) blocks of aerogel were cut out of one larger block, one might imagine the possibility that the four "smooth" block corners actually corresponded to the same point of the large block. (The fact that the top and bottom surfaces as well as two adjacent sides of each small block are rough indicates that this might have happened, *i.e.* that the smooth surfaces actually came from cutting the large block in four. See also the figure in footnote 5.) If this is the case, then we might expect two pairs of blocks to have equal α's and two pairs to have inverse α's, at least in the i regions. If the blocks, numbered as in footnote 5, were not moved after being cut, we would have $\alpha_1 = \alpha_4 = -\alpha_3$.

The results of averaging for each block separately (the solid colored lines in Figure 17) show that we may indeed have $\alpha_1 = \alpha_4$. Then, if the block cutting hypothesis is correct, the real value of n should be halfway between $\overline{n}_3$ and $\overline{n}_1 \approx \overline{n}_4$. A value of

$$n \approx \frac{1}{2}\left(\frac{1}{2}(\overline{n}_1 + \overline{n}_4) + \overline{n}_3\right) = 1.00950 \tag{52}$$

would then be a better guess than (51). However, the current evidence for block cutting as described above is *not* conclusive,[16] and the two values are certainly within each others error bounds, so we have kept (51).

3.5 Comparison to refraction

We recall that from the refraction method we obtained (Equation 17)

$$n_R = 1.00955 \pm 0.00015, \tag{54}$$

which agrees quite well with the interferometry value (Equation 51)

$$n_I = 1.00954 \pm 0.00025. \tag{55}$$

[16]Note that if the mean values are actually correct for each block (recall the calculation of these used $\alpha = 0$), and with $\partial n/\partial\alpha(0.7^\circ) \approx -0.0001$, a mid-way real value of n would actually require

$$\alpha_1 \approx \alpha_4 \approx 0.7^\circ, \quad \alpha_3 \approx -0.7^\circ. \tag{53}$$

This is a bit extreme and doesn't agree too well with refraction data....

These results were arrived at independently, using very different methods; their agreement is quite comforting (and perhaps even a little surprising). Combining them, we might obtain

$$n = 1.00955 \pm 0.00013, \tag{56}$$

where the error has been computed by the χ^2 method,

$$\delta n = \frac{1}{\sqrt{\frac{1}{\delta n_R^2} + \frac{1}{\delta n_I^2}}}. \tag{57}$$

However, it may at this point be wiser to simply leave them as separate results.

A Refraction data

The following tables give the raw refraction measurements taken. Recall that x (in centimeters) is a shift of the laser beam on the wall, and d is the distance to the wall.

γ	$x\ (x)$	$\delta x\ (x)$	$x\ (i)$	$\delta x\ (i)$	$x\ (m)$	$\delta x\ (m)$	$x\ (o)$	$\delta x\ (o)$
82.55	36.55	0.3	36.55	0.3	34.65	2.1	34.65	2.1
86.65	55.85	1.1						
85.35	43.55	2.1	43.55	2.1				
84.45	43.75	0.3	43.35	0.4	41.45	1.6	39.95	1.6
83.95	41.15	0.3	39.15	0.4	37.15	2.1	36.85	2.1
83.45	39.95	0.2	39.75	0.3	38.85	1.1	36.45	1.6
78.95	27.05	0.4	27.15	0.2	26.55	0.3	25.65	0.4
80.95	32.05	0.3	31.65	0.2	31.15	0.3	29.55	0.6
76.45	23.05	0.3	22.95	0.2	22.35	1.1	21.95	0.3
73.95	20.15	0.2	20.05	0.3	19.55	1.1	21.65	0.2
68.95	16.4	0.2	16.05	0.3	15.35	1.6	15.6	0.2
63.95	14.15	0.2	13.55	0.2	13.65	1.6	13.45	0.3
58.95	12.65	0.3	12.4	0.2	12.05	0.5	12.25	0.2
53.95	11.9	0.4	11.5	0.3	11.35	1.1	11.35	0.25
48.95	11.55	0.3	11.15	0.3	10.8	0.5	10.45	0.4
43.95	11.45	0.25	11.15	0.3	10.65	0.6	10.8	0.2
38.95	11.7	0.2	11.45	0.25	10.85	0.6	10.9	0.3
33.95	12.65	0.2	12.05	0.2	11.55	0.6	11.85	0.3
28.95	13.8	0.2	13.3	0.25	12.9	0.4	12.85	0.6
23.95	15.65	0.2	15.1	0.3	14.65	0.4	14.15	0.5
18.95	19.25	0.2	18.45	0.3	17.85	0.6	17.05	0.6
16.45	22.35	0.3	21.45	0.3	19.45	1.1	19.3	0.6
13.95	26.4	0.5	25.55	0.8	24.85	1.9	21.95	0.9
12.45	29.95	0.4	29.25	0.4	24.15	1.6	24.05	1.6
10.95	35.85	0.3	35.05	0.4	27.35	1.6	26.85	2.1
9.95	41.65	0.4	40.9	0.6	30.15	5.1	29.75	5.1
8.95	47.35	3.1	46.15	2.6	45.45	3.1	35.85	4.1

Table 3: Measured refraction data for **Block 1** ($d = 577.85$ cm)

γ	$x\ (x)$	$\delta x\ (x)$	$x\ (i)$	$\delta x\ (i)$	$x\ (m)$	$\delta x\ (m)$	$x\ (o)$	$\delta x\ (o)$
87.2	53.2	4.6	50.3	4.1	49.5	4.1	47.8	4.1
86.7	50.	2.1	46.1	1.6	45.25	1.1	45.1	1.1
85.2	43.9	1.1	42.3	1.6	39.2	0.6	38.7	0.6
83.7	38.8	0.5	37.8	2.1	34.8	0.8	33.9	1.1
81.7	32.5	0.6	31.2	1.1	29.5	1.1	29.4	0.6
78.2	25.4	0.3	24.5	0.8	23.5	1.1	23.2	0.4
75.7	21.8	0.3	21.1	0.6	20.	3.1	20.4	0.4
70.7	17.35	0.3	16.6	0.3	16.6	3.1	16.5	0.3
65.7	14.85	0.3	14.2	0.25	14.	2.1	13.9	0.2
60.7	13.25	0.2	12.6	0.2	12.7	1.1	12.4	0.3
55.7	12.3	0.3	11.7	0.3	11.8	1.6	11.4	0.4
50.7	11.6	0.3	11.2	0.3	11.5	1.1	11.2	0.3
45.7	11.6	0.3	11.	0.2	11.2	1.1	10.7	0.3
40.7	11.7	0.3	11.1	0.2	11.2	0.8	10.6	0.6
35.7	12.	0.3	11.55	0.4	11.2	0.8	11.15	0.4
30.7	13.2	0.3	12.3	0.5	12.2	1.1	12.15	0.4
25.7	14.9	0.3	14.35	1.6	13.5	1.1	13.3	1.6
20.7	17.7	0.35	17.	2.6	15.9	0.6	15.5	2.1
18.2	21.5	1.1	19.25	1.6	17.8	1.1	17.	1.6
15.7	22.7	1.1	21.8	2.1	20.	1.6	18.7	3.1
14.2	25.25	1.1	23.5	1.6	22.3	2.6	20.	5.1
12.7	28.8	2.6	26.5	1.6	26.5	3.1	22.5	5.1
11.2	32.5	3.1	30.9	2.6	30.2	3.1	28.5	4.1
10.2	37.5	3.1	35.5	3.1	34.6	3.1	34.4	3.1

Table 4: Measured refraction data for **Block 3** ($d = 579.12$ cm)

γ	$x\ (x)$	$\delta x\ (x)$	$x\ (i)$	$\delta x\ (i)$	$x\ (m)$	$\delta x\ (m)$	$x\ (o)$	$\delta x\ (o)$
48.4	11.2	0.2	11.25	0.3	10.95	0.3	10.8	0.3
53.4	11.7	0.2	11.9	0.2	10.75	0.3	11.2	0.4
58.4	12.35	0.2	12.3	0.2	11.6	0.4	11.7	0.5
63.4	13.8	0.3	13.45	0.2	13.	0.5	13.3	0.6
68.4	16.1	0.4	15.85	0.2	15.05	0.4	14.85	0.8
73.4	19.7	0.4	19.3	0.2	18.55	0.6	17.8	1.6
76.4	23.35	0.35	22.7	0.3	22.25	0.35	20.55	2.1
79.4	28.2	0.4	27.5	0.4	26.75	0.4	23.6	2.1
81.4	33.1	0.6	32.	0.6	31.3	0.6	31.6	0.6
83.4	38.5	1.1	38.3	1.1			38.2	0.6
84.9	44.85	2.1	43.9	1.1			43.4	1.1
86.4	52.8	2.1	52.8	2.1			52.6	2.1
87.4			59.4	2.1	59.4	2.1		
43.4	11.2	0.25	11.25	0.25	10.6	0.8	11.2	0.25
38.4	11.5	0.2	11.5	0.2	11.25	0.2	11.55	0.4
33.4	12.3	0.2	12.3	0.2	11.55	0.3	11.6	0.6
28.4	13.45	0.35	13.3	0.2	12.8	1.6	13.	0.6
23.4	15.6	0.35	15.4	0.2	15.15	1.1	14.7	0.7
18.4	19.15	0.3	18.8	0.3	18.2	2.1	17.4	1.1
13.4	26.6	0.3	26.	0.2	25.35	0.25	24.35	1.6
8.4	52.6	0.8	50.6	1.1	49.4	1.1	48.6	1.1
10.9	34.1	0.3	33.55	0.3	33.	0.4		

Table 5: Measured refraction data for **Block 4** ($d = 579.12$ cm)

We also show the results of some alternative computations, as described in Section 2.

Block	**Series**	$\overline{\mathbf{n}}$	$\overline{\alpha}$ (radians)	$\overline{\mathbf{d}\eta_\mathbf{0}}$ (radians)	**min** $\chi^\mathbf{2}$
1	x	1.00937 ± 0.000016	0.0032 ± 0.0005	0.00366	34.24
	i	1.00957 ± 0.000018	0.0018 ± 0.0007	0.00366	78.73
	m	1.00947 ± 0.000047	-0.0171 ± 0.0036	0.00366	18.40
	o	1.00963 ± 0.000033	-0.0337 ± 0.0033	0.00366	220.72
	combined	1.00961 ± 0.000011	0.0028 ± 0.0004	0.00366	652.19
3	x	1.01048 ± 0.000037	-0.0483 ± 0.0029	-0.02164	21.17
	i	1.00989 ± 0.000046	-0.0449 ± 0.0042	-0.02164	6.48
	m	1.00940 ± 0.000087	-0.0394 ± 0.0058	-0.02164	5.96
	o	1.00958 ± 0.000045	-0.0422 ± 0.0058	-0.02164	21.74
	combined	1.00997 ± 0.000023	-0.0404 ± 0.0020	-0.02164	328.23
4	x	1.00969 ± 0.000025	-0.0060 ± 0.0006	0.00157	5.43
	i	1.00957 ± 0.000021	-0.0069 ± 0.0006	0.00157	17.51
	m	1.00923 ± 0.000032	-0.0039 ± 0.0008	0.00157	11.92
	o	1.00938 ± 0.000056	-0.0073 ± 0.0015	0.00157	15.12
	combined	1.00953 ± 0.000014	-0.0061 ± 0.0004	0.00157	159.08

Table 6: Optimized values of n, α, and $d\eta_0$, using the full set of data

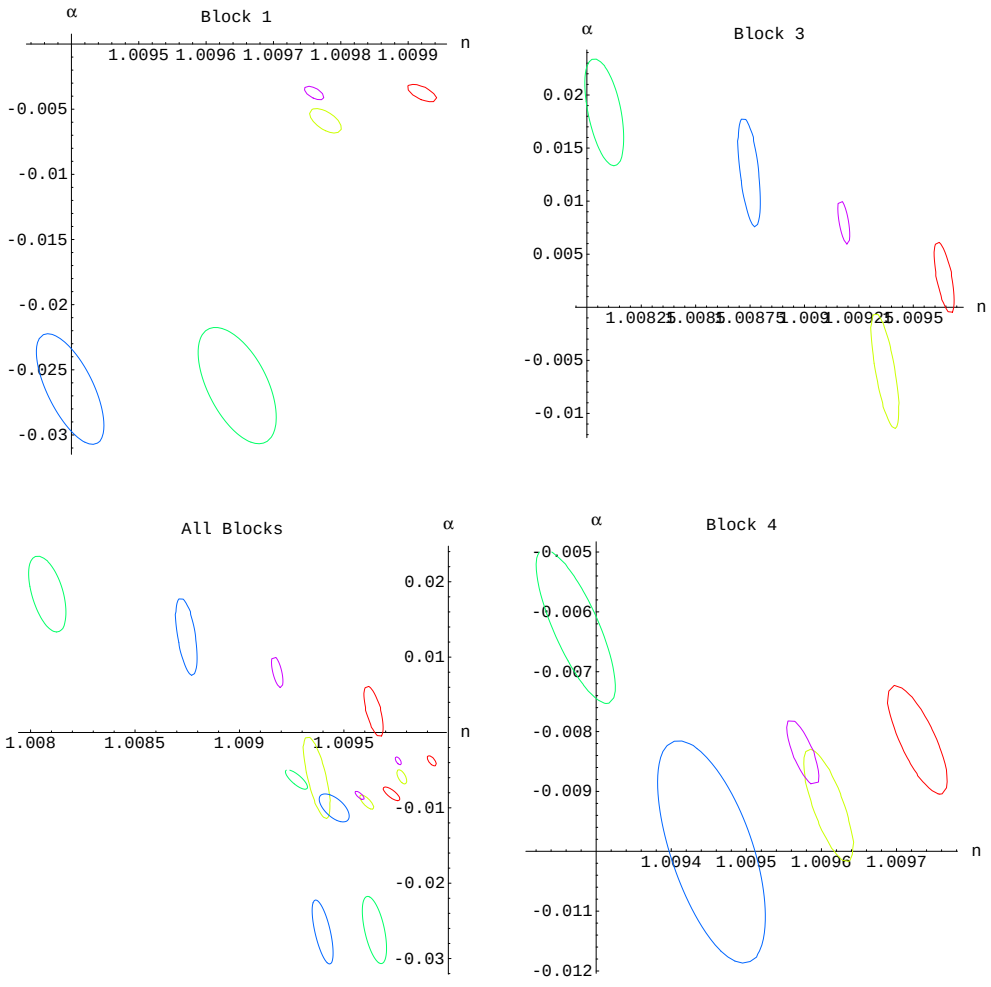

Figure 18: 1-sigma error bounds, fixing $d\eta_0 = 0$.

Block	**Series**	**n**	α (radians)	**min χ^2**
1	x	1.00992 ± 0.000016	-0.0038 ± 0.0005	42.59
	i	1.00978 ± 0.000019	-0.0059 ± 0.0007	73.18
	m	1.00965 ± 0.000047	-0.0261 ± 0.0022	19.06
	o	1.00940 ± 0.000037	-0.0264 ± 0.0020	20.08
	combined	1.00976 ± 0.000011	-0.0037 ± 0.0004	592.20
3	x	1.00964 ± 0.000035	0.0028 ± 0.0025	31.22
	i	1.00937 ± 0.000044	-0.0058 ± 0.0031	12.60
	m	1.00808 ± 0.000082	0.0186 ± 0.0037	38.14
	o	1.00875 ± 0.000043	0.0129 ± 0.0040	164.89
	combined	1.00918 ± 0.000022	0.0080 ± 0.0016	668.34
4	x	1.00973 ± 0.000025	-0.0081 ± 0.0006	7.88
	i	1.00961 ± 0.000021	-0.0092 ± 0.0006	15.82
	m	1.00927 ± 0.000032	-0.0062 ± 0.0007	12.86
	o	1.00945 ± 0.000055	-0.0099 ± 0.0011	10.65
	combined	1.00958 ± 0.000014	-0.0083 ± 0.0003	151.99

Table 7: Optimized values of n and α, fixing $d\eta_0 = 0$

B Interferometry data

Here we document the data measured for interferometry. Note that q really refers to Δq, a change in fringes, and that what we call Δd is often referred to in the above discussion as simply d. We always have $\delta d = 4$ μm and $\lambda_0 = 632.8$ nm; and for all calculations we assume $\alpha = 0 \pm 0.7$ degrees (as explained above).

$\mathbf{q}$	$\delta\mathbf{q}$	$\mathbf{d_f}$ (μ)m	$\mathbf{d_i}$ (μ)m	$\mathbf{\Delta d}$	γ	$\delta\gamma$
25	0.4	5576	5130	446	47.1	0.36
50	0.5	6862	5943	919	47.1	0.36
100	2	8562	6953	1609	47.1	0.36
50	0.5	9443	8600	843	47.1	0.36
50	1	10900	10050	850	47.1	0.36
50	0.6	11671	10900	771	47.1	0.36
10	0.3	11839	11677	162	47.1	0.36
50	0.3	11934	11164	770	47.1	0.36
100	0.7	12782	11164	1618	47.1	0.36
50	0.3	13580	12782	798	47.1	0.36
50	1	14425	13580	845	47.1	0.36
100	1	6500	4950	1550	45	2
10	0.1	4950	4791	159	45	2
50	1	4351	3500	851	49.3	0.45
100	1	5134	3500	1634	49.3	0.45
50	1	13500	12639	861	45.2	0.45

Table 8: Block 1 measurements

$\mathbf{q}$	$\delta\mathbf{q}$	$\mathbf{d_f}$ (μ)m	$\mathbf{d_i}$ (μ)m	$\mathbf{\Delta d}$	γ	$\delta\gamma$
50	1	3986	3120	866	44.9	0.36
50	1	4821	3986	835	44.9	0.36
10	0.12	5042	4880	162	44.9	0.36
50	0.7	5678	4880	798	44.9	0.36
25	0.2	6161	5719	442	44.9	0.36
15	0.2	7679	7435	244	44.9	0.36
25	0.5	8721	8255	466	44.9	0.36
100	1	5164	3500	1664	45	2
75	1	13009	11750	1259	44.7	0.45
100	1	7229	5500	1729	44.7	0.45

Table 9: Block 3 measurements

$\mathbf{q}$	$\delta\mathbf{q}$	$\mathbf{d_f}$ (μ)m	$\mathbf{d_i}$ (μ)m	$\mathbf{\Delta d}$	γ	$\delta\gamma$
100	1	7881	6358	1523	47.15	0.36
50	0.3	8675	7875	800	47.15	0.36
50	0.3	9493	8675	818	47.15	0.36
50	0.65	10352	9493	859	47.15	0.36
50	0.6	11209	10352	857	47.15	0.36
50	1	12401	11571	830	47.15	0.36
50	0.5	12791	12000	791	47.15	0.36
100	2	4677	3000	1677	45	2
100	1	6373	4677	1696	45	2
100	0.5	13500	11820	1680	45.4	0.45
100	0.5	13853	12182	1671	45.4	0.45
50	0.5	13853	12999	854	45.4	0.45
50	1	10997	10148	849	45.4	0.36
100	0.5	8821	7337	1484	45.4	0.45
50	0.5	6500	5665	835	45.4	0.45
50	1	5665	4836	829	45.4	0.45
100	1	7637	5937	1700	44.5	0.45
100	2	9278	7633	1645	44.5	0.45
100	2	7640	9278	1638	44.5	0.45
100	1	10982	9283	1699	44.5	0.45
100	2	9297	10982	1685	44.5	0.45
100	1	10837	9190	1647	44.5	0.45
100	2	12467	10837	1630	44.5	0.45
100	0.5	13605	11940	1665	44.5	0.45

Table 10: Block 4 measurements

C Acknowledgements

The author wishes to thank his advisor, Kirk McDonald of Princeton University, for posing the initial problem of measuring the index of an aerogel, and for his guidance throughout the undertaking.